ZnO/reduced graphene oxide nanocomposite with synergic enhanced gas sensing performance for the effective detection of NO$_2$ at room temperature

Junfeng Lu · Donglin Li · Xianjia Chen · Xiaolin Peng · Jing Li · Yanting Yang · Bo Hong · Xinqing Wang · Dingfeng Jin · Hongxiao Jin

Abstract Here, we demonstrate room temperature NO$_2$ sensors based on ZnO/rGO nanocomposites by a facile hydrothermal method. The ZnO nanoparticles (20 ~ 50 nm) were wrapped by film-like rGO with different contents (0.5, 1.0, 2.0, 3.0 wt %). They all exhibit p-type sensing toward NO$_2$ at room temperature. The content of rGO shows an obvious effect on the sensing properties. The ZnO NPs-1% rGO has a high response of 5.21 to 10 ppm NO$_2$ with a response/recovery time of 198/144 s. The sensing mechanism is discussed. The gas-sensitive properties are derived from the strong synergistic effect between the smaller particles of ZnO and rGO.

Keywords Synergistic effect · Gas sensing · p–n junction · Reduced graphene oxide · ZnO · Nanostructures

J. Lu · D. Li · X. Chen · X. Peng · J. Li · Y. Yang ·
B. Hong · X. Wang · D. Jin · H. Jin (✉)
Zhejiang Province Key Laboratory of Magnetism, College
of Materials and Chemistry, China Jiliang University,
Hangzhou 310018, People's Republic of China
e-mail: hxjin@cjlu.edu.cn; hxjin5704@qq.com

J. Lu
e-mail: lu418jun513@163.com

D. Li
e-mail: 2933406014@qq.com

X. Chen
e-mail: 806694723@qq.com

X. Peng
e-mail: pxlqingliu@cjlu.edu.cn

J. Li
e-mail: jingli@cjlu.edu.cn

Y. Yang
e-mail: 14a0505087@cjlu.edu.cn

B. Hong
e-mail: bohong@cjlu.edu.cn

X. Wang
e-mail: wxqnano@cjlu.edu.cn

D. Jin
e-mail: dfjin@cjlu.edu.cn

Introduction

With the acceleration of modern industrial processes, many toxic gases are being released directly into the air. Nitrogen dioxide (NO$_2$), a common pollution emission released by fossil fuel combustion, power plants, and automotive engines, is harmful to the environment and human health [1, 2]. To effectively monitor air quality and protect human safety, it is of great significance to develop NO$_2$ gas sensors with high sensitivity, low detection limit, and high selectivity.

Metal oxide semiconductors, such as SnO$_2$, ZnO, TiO$_2$, and CuO, are extensively used as gas sensors to detect hazardous gas leaks and monitor air pollutants. Among these gas sensing materials, ZnO has been widely studied for its stable physicochemical

properties, controlled morphology and microstructure, optical activity, nontoxicity, and good gas-sensitive properties. It is an important direct wide band gap (~ 3.37 eV) semiconductor metal oxide after SnO_2. However, the performance of most reported gas sensors based on ZnO is not applicable at room temperature. This kind of gas sensor requires sufficient reaction activation energy between the target gas molecules and the oxygen ions adsorbed on the surface. The working temperature is usually higher than 200 °C, which limits the application [3–5].

Graphene has attracted extensive interest due to its high surface area (2630 m^2g^{-1}), electron mobility (200,000 cm^{-1} $V^{-1}S^{-1}$), electrical conductivity (5000 W/mK), etc. [6] The high electron mobility and excellent electrical conductivity create extremely low detection limits in gas sensing [7, 8]. Tuning the semiconductor properties by adding graphene is a promising strategy for the fabrication of room temperature sensing materials. Although the sensors prepared from graphene can achieve the detection of NO_2 gas at room temperature, the van der Waals force between graphene and gas is weak, which will directly lead to the drawbacks of gas sensors from pure graphene [9–11]. Therefore, reduced graphene oxide (rGO), a form of graphene produced by the reduction of graphene oxide, which contains many defects, is preferred for sensing studies [12–14]. rGO has more dangling bonds and defects than graphene, which is good for the adsorption of gas and the formation of heterojunction with metal oxides.

To obtain a room-temperature NO_2 sensor based on metal oxide/graphene nanocomposites with low sensitivity, short response time, and response recovery time, many recent efforts have been devoted to the controllable synthesis of metal oxides with confined sizes and desired morphologies in nanocomposites [15–17]. For example, rGO-conjugated Cu_2O nanowire monocrystals were hydrothermally fabricated. They exhibited high sensitivity toward NO_2 at room temperature owing to the unique nanowire-assembled mesoporous structures. Wang et al. used a microwave-assisted hydrothermal method to uniformly load 3-nm SnO_2 nanoparticles on rGO [18, 19]. The composite showed significant gas-sensitive properties, especially for NO_2, with a high response, fast response, and good recovery. It has six times the response of SnO_2 at 75 °C for 350 ppb NO_2. The response to 50 ppb NO_2 still has a response, so the composite material has many advantages over a single gas-sensitive material.

Herein, ZnO/rGO with different rGO ratios was synthesized by a hydrothermal method. The characterization results showed that rGO influenced the agglomeration of ZnO particles. ZnO and rGO were hybridized to construct heterojunctions and nanostructures. Among the ZnO/rGOs, ZnO NPs-1% rGO exhibited the best room-temperature NO_2 gas-sensitive performance. The excellent gas-sensitive properties of the composites are derived from the strong synergistic effect between the smaller particles of ZnO and rGO. In addition, the mechanism of sensing NO_2 gas by the ZnO/rGO heterostructure is discussed.

Experimental section: Materials and methods

Chemicals

Commercial grade ZnO dispersion was purchased from Zhejiang Zhongliang Chemical Reagent Co., Ltd. Graphite powder was purchased from Nanjing Xianfeng Nanomaterials Technology Co., Ltd. Potassium permanganate, hydrogen peroxide, and zinc nitrate were purchased from Shanghai Lingfeng Chemical Reagent Co., Ltd. Absolute ethanol and hydrochloric acid were purchased from Aladdin Reagent Co., Ltd. The corresponding solutions were prepared using distilled water. All required replacement parts were analytically pure and used directly without any further purification.

Preparation of graphene oxide

Graphene oxide (GO) nanosheets were synthesized via Hummer's method from graphite powder. First, 3.0 g of graphite powder was dissolved in 69 mL of sulfuric acid and vigorously stirred for 10 min. Then, 1.5 g of sodium nitrate was added to the mixture to obtain a homogeneous solution, which was kept at 0 °C during this process. Then, 9.0 g of potassium permanganate was added to the mixture, vigorously stirred for 3 h, and continuously stirred for another 6 h at 35 °C. Then, 550 mL distilled water and 20 mL H_2O_2 were added and continuously stirred for 2 h. Finally, the samples were repeatedly washed with distilled water to pH = 7.

To completely remove metal ions, the sample was dialyzed for 2 weeks. A graphene oxide/water dispersion (5 mg/mL) was made from freeze-dried GO powder for further use [20, 21].

Synthesis of ZnO/rGO

One gram of nano ZnO was added to 20 mL of deionized water with stirring; desired amounts of graphene oxide dispersion were added dropwise to the ZnO dispersion, forming a homogeneous ZnO/GO dispersion with 0 %, 0.5 %, 1 %, 2 %, and 3 % GO in mass ratio. The dispersion was treated with ultrasonication for 0.5 h. Then, it was put into a Teflon-lined stainless steel autoclave and heated at 180 ℃ for 6 h. After that, GO transformed to rGO, and the ZnO/rGO composite formed simultaneously. The ZnO/rGO was centrifuged, washed with distilled water and ethanol, and freeze dried. Samples were labeled ZnO NPs and ZnO NPs-x% rGO (x = 0.5, 1, 2, and 3) according to the GO mass ratio.

Material characterization

X-ray diffraction (XRD) patterns were recorded on a diffractometer (D8-ADVANCE, Bruker, Germany) with Cu Kα radiation ($\lambda = 1.5418$ Å) to analyze the phase and crystallinity of the composite materials. The morphology and microstructure of the as-prepared samples were characterized by field-emission scanning electron microscopy (FESEM, S-4800, Hitachi Ltd., Japan) and high-resolution transmission electron microscopy (TEM, JEM-2100, JEOL, Japan). X-ray photoelectron spectroscopy (XPS) was conducted on a spectrometer with an Al Kα X-ray source (Thermo ESCALAB 250 Xi, USA). The BET surface areas of the materials were determined using a nitrogen adsorption analyzer (Micromeritics ASAP 2020, Merrick, USA). Raman spectra (HORIBA, LabRAM HR, France) were recorded on a laser confocal microscopy Raman spectrometer. Ultraviolet visible (UV–Vis) diffuse reflectance spectroscopy (DRS) was performed using a UV–Vis spectrophotometer (Shimadzu UV-2600, Japan) and $BaSO_4$ as the reflectance standard. Photoluminescence spectra (PL) were recorded on a fluorescence spectrometer (HORIBA, Quanta Master 8000, Canada).
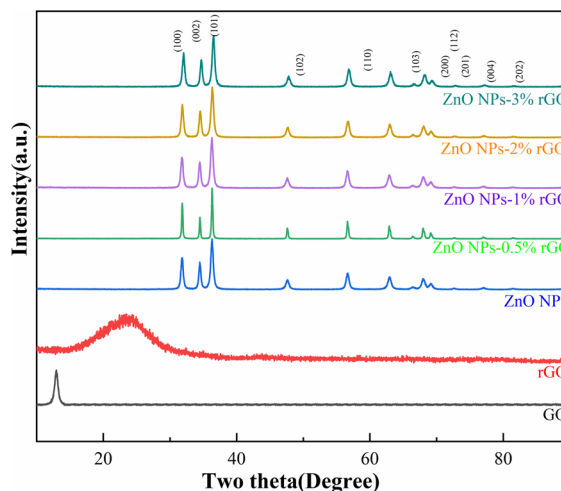

Fig. 1 XRD patterns of GO, rGO, and ZnO/rGO

Gas sensing measurements

The ZnO/rGOs were first mixed with a small amount of deionized water to form the paste in an agate mortar. Then, it was coated on an alumina substrate with two Ag-Pd electrodes to form a sensing film. The samples were aged in a muffle furnace at 200 ℃ for 6 h. The gas sensing property was measured on a CGS-4TPS system (Alite Technology Co. Beijing, China). Before the measurements, the chamber was purged with pure dry air until stable resistance was obtained, which was defined as the background gas. Then, in a measurement, the sensors were alternately exposed to different gases for the response process and to the pure dry air flow for the recovery process. The sensitivity (S) of the sensor is defined as Ra/Rg, where Ra is the initial resistance in dry air, and Rg is the resistance of the sensitive film after exposure to an NO_2 atmosphere. For the p-type sensor, the resistance is decreased upon NO_2 exposure (S > 1). The response time is defined as the time required until 90% of the whole response is reached, while the recovery time denotes the time needed until 90% of the baseline sign is recovered.

Results and discussion

Characterization

The structure and phase of the samples were examined by powder X-ray diffraction (XRD). As shown in

Fig. 1, the XRD pattern of GO shows an intense peak (001) at 10.6° with a d-spacing of 0.8336 nm. After the reduction of GO to rGO by hydrothermal treatment, the peak in GO disappears, and a broad peak appears. The broad peak suggests a poorer ordering of the graphene sheets along their stacking direction than that of GO. The variation in diffraction peaks revealed successful transformation from GO to rGO via the same hydrothermal treatment as the synthesis of ZnO/rGO hybrids. The XRD patterns of ZnO and ZnO/rGO clearly demonstrate the stability of the ZnO nanoparticles toward hydrothermal treatment because the representative sharp peaks agree well with those from the standard JCPDS card (No. 79–206). In addition, the diffraction peaks of rGO were not observed among the ZnO/rGO samples, which may be related to the low doping concentration of rGO.

The morphology and microstructure of the ZnO and ZnO/rGOs were characterized by SEM, TEM, and HRTEM. Figure 2 displays the SEM and TEM images of pure ZnO nanoparticles and ZnO NPs-1% rGO. The size (20–50 nm) and shape of pure ZnO are not perfectly uniform (Fig. 2a and b). The diameter of the ZnO nanoparticles remained unchanged after thin film–like rGO wrapped the ZnO nanoparticles through hydrothermal synthesis (Fig. 2c and d). However, the sample shows a kind of lamellar agglomeration morphology (Fig. 2c). This is due to the interaction of ZnO with hydrophilic GO sheets

before hydrothermal reduction. The HRTEM images (Fig. 3) of ZnO NPs-1% rGO display more details of the materials. The lattice fringes with spacings of 0.26 nm and 0.19 nm (Fig. 3d) are attributed to the (002) and (102) crystal planes of hexagonal ZnO. This is consistent with the XRD results. In the HRTEM images, we also observed that ZnO is well combined with rGO (Fig. 3c).

The XPS spectra of the samples (Fig. 4) show the presence of carbon, oxygen, and zinc elements. In the Zn2p region (Fig. 4b), $Zn2p_{1/2}$ and $Zn2p_{3/2}$ peaks at binding energies of approximately 1045.0 and 1022.0 eV were observed, which are ascribed to spin–orbit coupling of Zn2p with a ΔE (spin–orbit splitting) of approximately 23.1 eV. It is worth noting that the Zn2p peaks are shifted to higher energy positions with the doping of rGO. The formation of a higher energy for Zn is due to electrostatic repulsive interactions among O with a negative charge in the lattice. The O1 s signals (Fig. 4c) are quite asymmetric and can be decomposed into three Gaussian peaks at 530, 531, and 532.33 eV, corresponding to different oxygen species in the sample. The most prominent lowest binding energy peak is attributed to the lattice oxygen (O_L) of ZnO, and the middle binding energy peak is linked to surface hydroxyls in the oxygen-deficient regions (OH), whereas the highest binding energy peak is associated with the chemisorbed or dissociated oxygen species on the surface

Fig. 2 SEM of ZnO NPs (**a**); TEM of ZnO NPs (**b**); SEM of ZnO NPs-1% rGO (**c**); TEM of ZnO NPs-1% rGO (**d**)
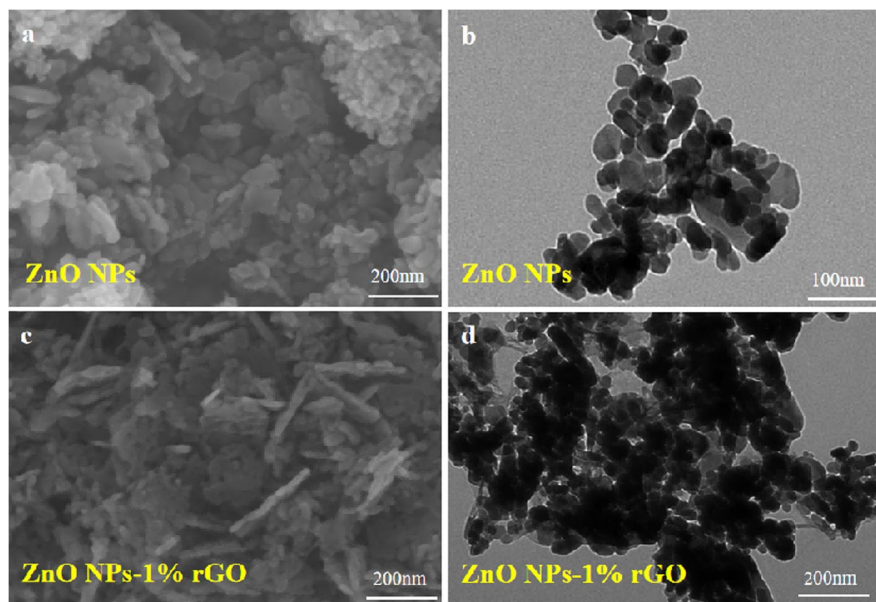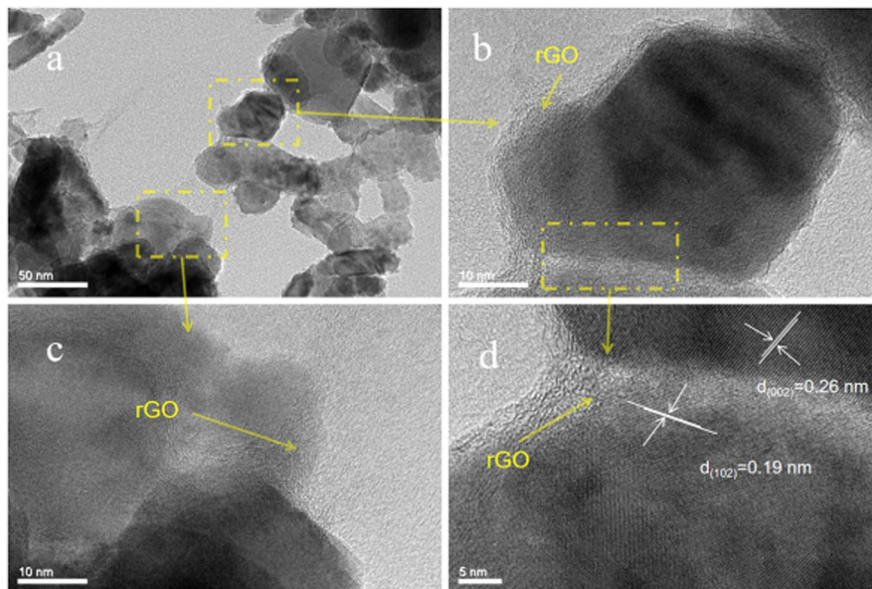
Fig. 3 a–d HRTEM image of ZnO NPs-1% rGO

of the sample. In the C1 s region (Fig. 4d and e), the spectra of GO, rGO, and ZnO/rGO can be subdivided into three peaks at 284, 286, and 289 eV corresponding to the C–C/C=C (sp^2/sp^3 carbon atom), C-O (epoxy/alkoy), and C=O/C–O–C (carbonyl) functional groups of rGO. After the hydrothermal treatment of ZnO nanoparticles with GO dispersion, the intensity of the C-O peak decreases, and the C–C peak increases in all samples.

The physical nitrogen desorption curves of the five samples are shown in Fig. 5. According to the IUPAC classification, the adsorption isotherms of the samples in the figure are all type IV. With the increase in the rGO doping ratio, the specific surface area of the composites also increases, and the pore capacity and pore size are changed accordingly (Table 1). The main pore structure may be generated by the agglomerative accumulation of ZnO nanoparticles, and rGO acts as an isolation layer during its drying process, which can effectively prevent serious agglomeration during drying, leading to a high specific surface area. These hollow structures, also shown in SEM and TEM images, promote the diffusion of target gas molecules inside the material and improve the response and recovery ability of the gas sensing materials.

Raman spectroscopy is an effective and sensitive technique to characterize carbon-based materials. The ZnO/rGO composites exhibit two intensive peaks (Fig. 6), which correspond to the D and G bands. The D band at approximately 1340 cm^{-1} originates from the breathing mode of k-point phonons of the A1 g symmetry near the edges of graphitic structures, which increases with increasing defect density (local defects or disorder); the G band at approximately 1600 cm^{-1} belongs to the E$_{2g}$ mode of sp^2-hybridized carbon atoms (stacking nature) of the rGO species. The intensity ratio of the D band to the G band (I_D/I_G) is usually used as a parameter to evaluate the disorder and defect degree of various carbon materials; that is, the larger I_D/I_G is, the higher the disordering in the carbon materials. The I_D/I_G of ZnO/rGO composites is 1.03, 1.01, and 1.02 for ZnO NPs-1% rGO, ZnO NPs-2% rGO, and ZnO NPs-3% rGO, respectively, showing the similar in-plane crystallite size of ZnO/rGO samples [22]. The second-order D(2D) bands at approximately 2667 cm^{-1} and D+G bands at approximately 2918 cm^{-1}, belonging to rGO, were also observed in rGO and ZnO/rGO samples, further verifying the formation of rGO in the synthesis [23].

Figure 7a shows the UV–Vis absorption of the materials. Pure ZnO shows a strong band-to-band transition absorption peak at∼380 nm. No apparent absorption is observed in the visible light region. As a zero-gap semiconductor, graphene is a good light-absorbing material, so introducing rGO into ZnO can greatly enhance the adsorption in the visible light region and generate
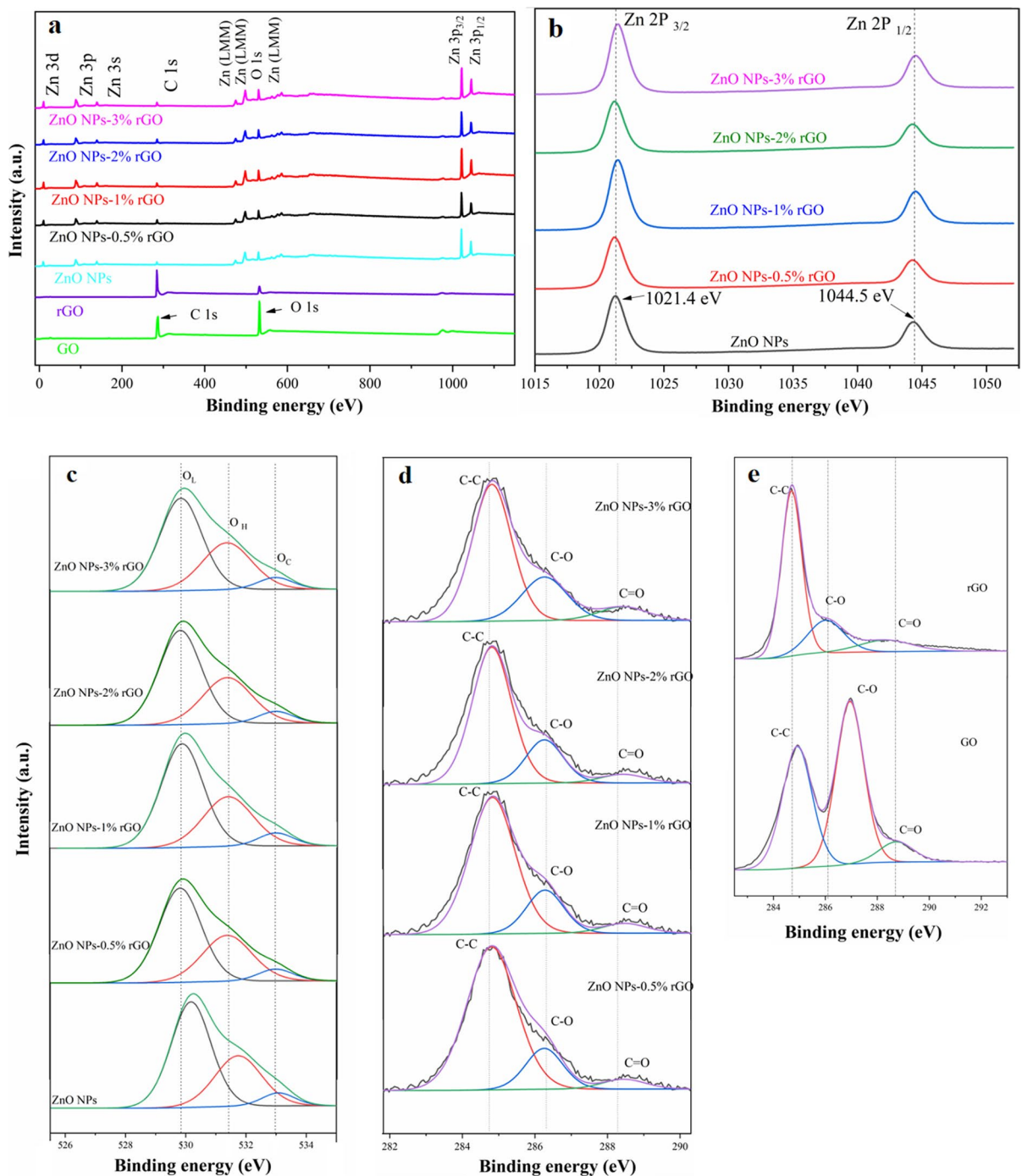
Fig. 4 XPS survey spectra of GO, rGO, ZnO, and ZnO/rGOs (**a**); magnified Zn 2p core level (**b**); deconvoluted high-resolution O1 s spectrum (**c**); deconvoluted high-resolution C1 s spectrum of (**d**) and (**e**)

an electronic energy level below the CB (conduction band) of ZnO. Meanwhile, the visible light absorption ability of ZnO/rGO can be effectively enhanced with the increase in the amount of rGO. The energy gap (E_g) is calculated with the formula for the near-edge optical absorption of semiconductors:
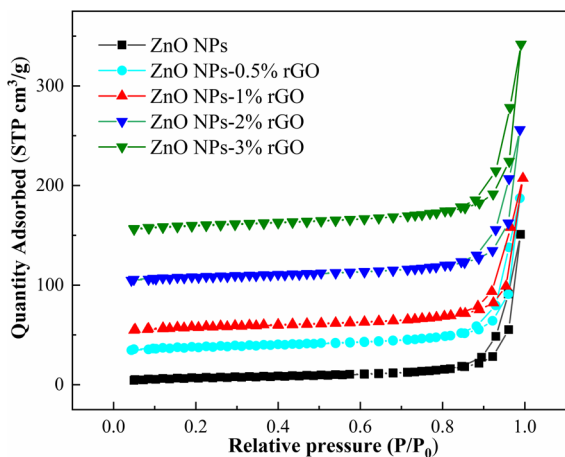
Fig. 5 Nitrogen adsorption–desorption isotherms of ZnO and ZnO/rGO composites

Table 1 Specific surface area and pore volume

Samples	BET surface area (m^2/g)	Pore volume (m^3/g)
ZnO NPs	26.1279	0.2335
ZnO NPs-0.5% rGO	28.3214	0.2384
ZnO NPs-1% rGO	30.7597	0.2433
ZnO NPs-2% rGO	31.2457	0.2414
ZnO NPs-3% rGO	37.5705	0.2966
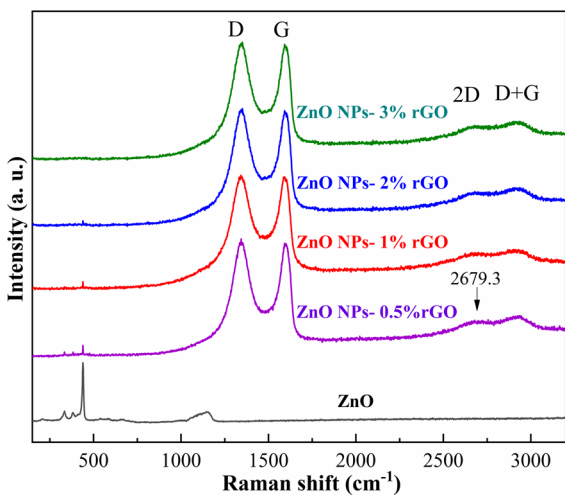
Fig. 6 Raman spectra of ZnO and ZnO/rGOs

$$(\alpha h v)^n = c_0 \times (h v - Eg) \tag{1}$$

where C_0 is a constant, $h\nu$ is the photon energy, Eg is the energy gap, and $n = 2$ for the direct band gap semiconductor [24]. As shown in Fig. 7c–g, the Eg value changed from 3.179 eV (ZnO NPs) to 3.212 eV (ZnO NPs-3% rGO) as the doping amount of rGO increased.

The photoluminescence (PL) spectra provide the separation and recombination information of the photoinduced electrons and holes in the materials. Figure 7b shows the PL spectra of pure ZnO and ZnO/rGO with an excitation wavelength of 325 nm at room temperature. All five materials showed a strong UV emission at a wavelength of 380 nm and a broad green emission band at 580 nm. The peak emission at 380 nm is the recombination of the charge carriers of materials, and the green emissions centered at 580 nm are from the surface defects of ZnO. In addition, the intensities of all ZnO/rGOs are weaker than those of pure ZnO, indicating that the fluorescence of the ZnO/rGO composites is quenched more efficiently than that of pure ZnO NPs. This result also suggested a strong interaction between ZnO and rGO, which indicated more separation of photoinduced electrons and holes by the addition of GO.

Gas sensing properties

The sensors were made by depositing the material dispersion on the microelectrode surface. Figure 8 shows the resistance of the ZnO-, ZnO/rGO-, and rGO-based sensors at room temperature. The sensor based on ZnO shows the largest resistance. It behaves almost insulatively at room temperature. As an n-type sensor shows an increase in resistance in NO_2 gas, it is difficult to test the sensing performance at room temperature. The best working temperature is usually above 150° [25]. rGO exhibits the lowest resistance because of its excellent electrical conductivity. As a p-type sensor showing a decrease in resistance in NO_2 gas, the sensor based on rGO exhibits a weak response [26]. With the combination of ZnO and rGO, sensors based on ZnO/rGO show a medium resistance with p-type sensing. The higher the ratio of rGO in the hybrid materials, the lower the resistance was observed.
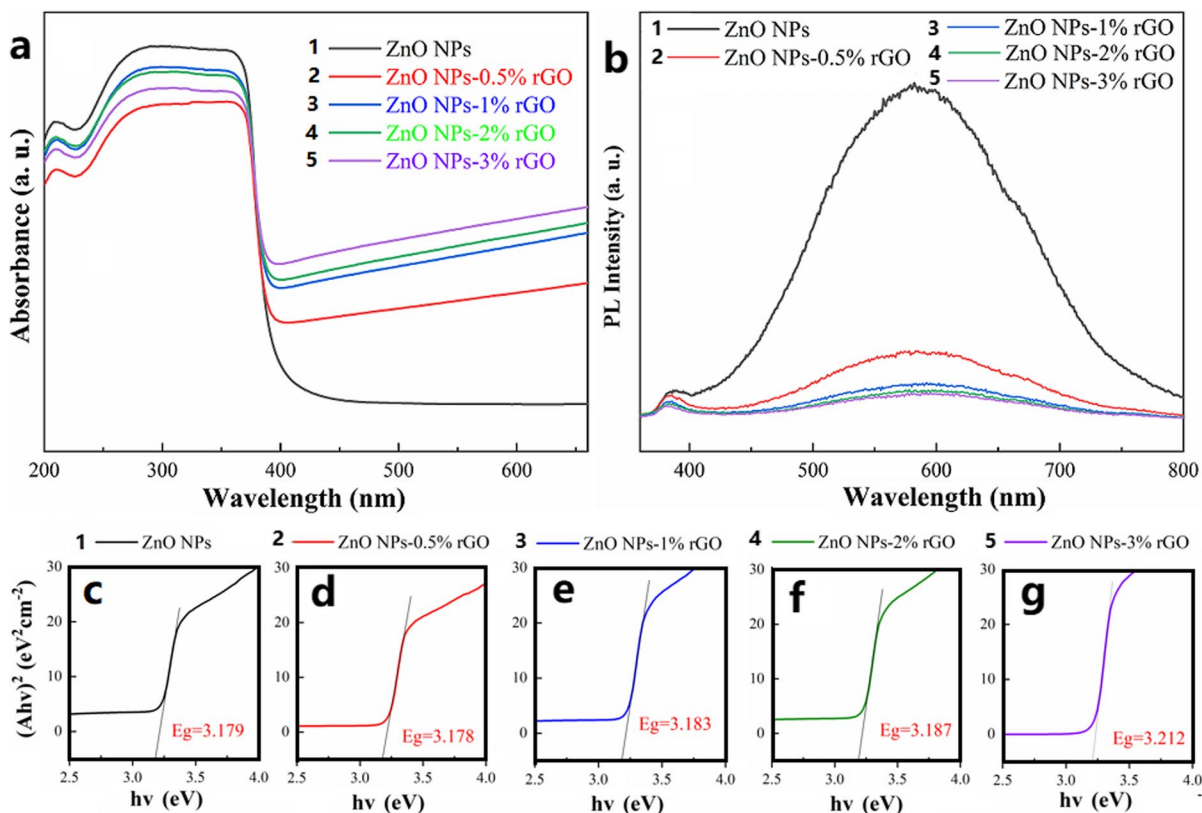
Fig. 7 UV–Vis absorption spectroscopy (**a**) and PL spectra (**b**). Plot of $(\alpha h\nu)^2$ vs. Hν (**c–g**) of ZnO and ZnO/rGOs
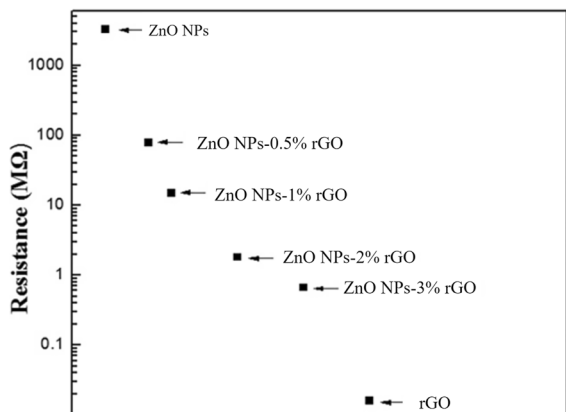

Fig. 8 Resistance of ZnO and ZnO/rGO composites

Gas sensors based on pure ZnO or rGO show no or a weak response in NO_2, so only ZnO/rGO-based sensors were tested at room temperature. The sensors were first exposed to a range of NO_2 gas concentrations (5~30 ppm). They exhibit a stable

signal with a good p-type response (Fig. 9a). The maximum gas response is achieved at a reduced graphene oxide (~1%) content (ZnO NPs-1% rGO). This may be due to the synergistic interaction between ZnO and rGO in nanocomposites, where ZnO nanoparticles are the non-negligible sensing material involved in gas adsorption and interaction with NO_2, while rGO with excellent transport capacity provides more electrical channels for the nanocomposites, directing current through the nanocomposites and electrodes to obtain a response and improved sensing. Figure 9b shows the dynamic response recovery curves of the ZnO NPs-1% rGO composites for different concentrations of NO_2 gas. The gas response at room temperature is a relatively slow process, but all the samples have a good response, and the baseline can roughly recover to the initial value. As shown in Fig. 9d, the response time and recovery response time of ZnO NPs-1% rGO are 198 s and 144 s, respectively. Figure 9c shows the results of 3 consecutive cycles of ZnO
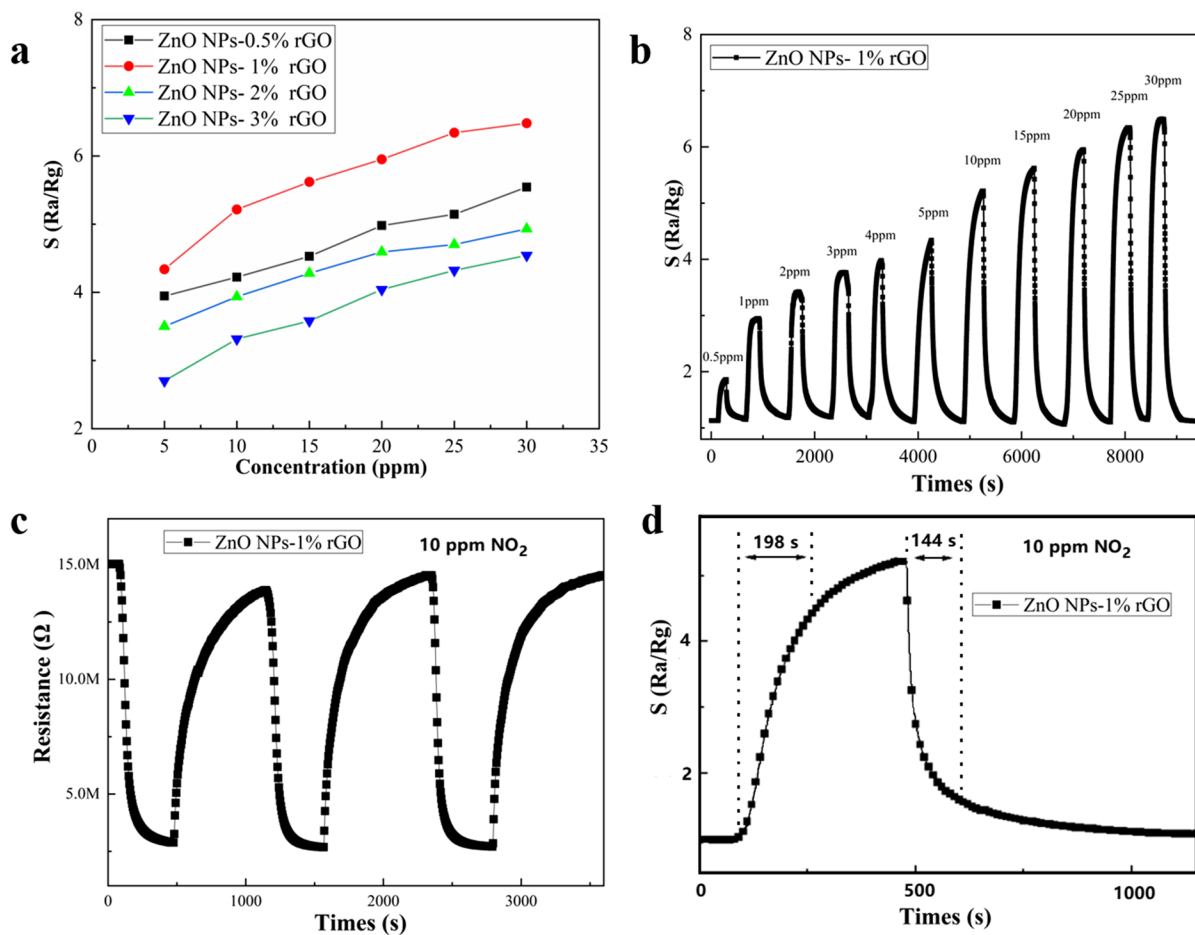
Fig. 9 Response of the sensors based on ZnO/rGOs (**a**); dynamic response curves of the sensor based on ZnO NPs-1% rGO toward NO$_2$ at concentrations ranging from 0.5 to 30 ppm (**b**); reproducibility (**c**), recovery and response time (**d**) of the sensors based on ZnO NPs-1% rGO; the response curves toward 10 ppm NO$_2$

NPs-1% rGO. ZnO/rGO can be adjusted and recover to its initial state without external heat or illumination, and there is no drift in the baseline after recovery.

The signal-to-noise ratio method was used to quantify the detection limit (LOD) of NO$_2$ [22]. The LOD can be calculated by Formula (2) below:

$$\text{LOD} = 3 \times \frac{RMS_{nosie}}{K} \tag{2}$$

where RMS$_{noise}$ is the root mean square noise and "K" is the slope value in the linear fitting of the response ($y = 0.585x + 2.022$). The sensor noise can be calculated by the relative resistance variation from the average resistance measured. Thirty Ra values were taken to calculate the standard deviation before exposure to NO$_2$ by Formula (3).

$$\text{RMS}_{nosie} = \sqrt{\frac{\sum_{i=1}^{N}(R_i - \overline{R})^2}{N}} \tag{3}$$

where R_i is the randomly selected Ra value and R is the average resistance of the thirty randomly selected Ra values. In this work (Fig. 10), the RMS$_{noise}$ of ZnO NPs-1% rGO is calculated to be 0.000869, and the LOD is 4.4 ppb.

To check the effect of humidity on sensing performance, the sensitivities of the ZnO NPs-1% rGO sensor were investigated at 10%, 25%, 50%, and 75% relative humidity (%RH) under 10 ppm NO$_2$ gas (Fig. 11). The influence of the humidity obviously
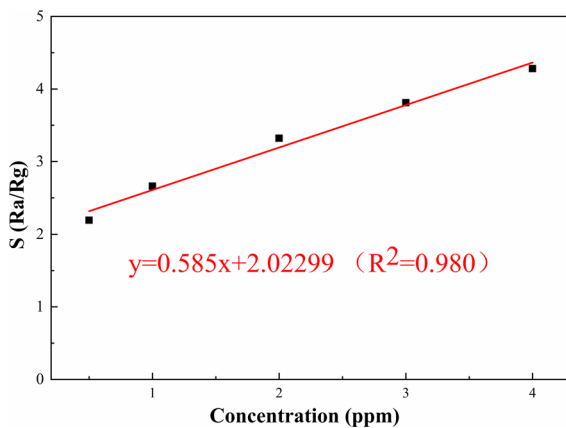
Fig. 10 The fitting curve of ZnO NPs-1% rGO to 0.5–4 ppm NO$_2$ at room temperature
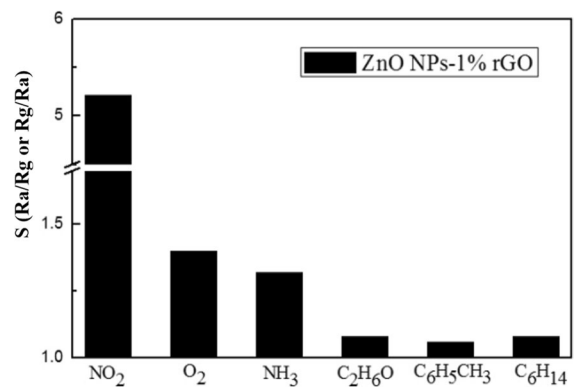

Fig. 12 Responses of the ZnO NPs-1% rGO composites to 10 ppm NO$_2$ and other gases (oxygen, ammonia, ethanol, toluene, n-hexane)
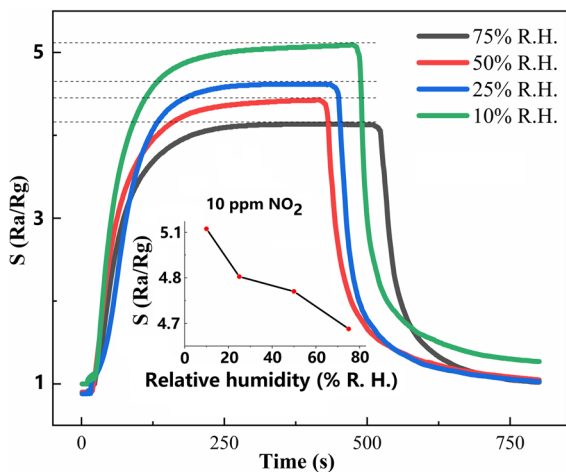

Fig. 11 The dynamic response curves of ZnO NPs-1% rGO to 10 ppm NO$_2$ under various relative humidities at room temperature

Fig. 13 Stability of the ZnO NPs-1% rGO composites when exposed to 5 ppm NO$_2$ gas at room temperature (25 °C)

occurs from 10 to 75%, where there is a relatively obvious variation in the sensor response. Under 75% RH, the response drops to ~75% compared with the response under 10% RH.

The cross-sensitivity of the ZnO NPs-1% rGO sensor toward other gases, such as toluene, ethanol, oxygen, ammonia, and n-hexane, at 10 ppm was tested at room temperature (Fig. 12). The ZnO NPs-1% rGO exhibits a high response toward NO$_2$, a weak response to ammonia and oxygen, and almost no response to toluene, hexane, and ethanol gases, suggesting that the ZnO/rGOs have good selectivity to NO$_2$. The
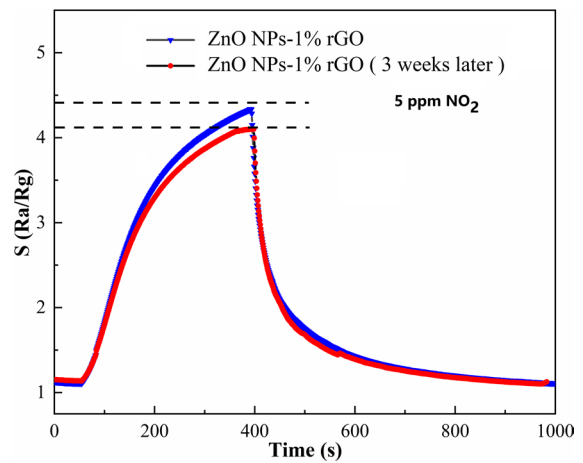
remarkable selectivity to NO$_2$ of the ZnO/rGOs could be related to the selective and high NO$_2$ adsorption ability of the material at room temperature.

In addition, the long-term stability of the ZnO NPs-1% rGO sensor was tested with 5 ppm NO$_2$ for 20 days (Fig. 13). The response of the ZnO NPs-1% rGO gas sensor remained relatively stable (from 4.45 to 4.18).

A comparison of NO$_2$ sensing performance at room temperature between the present ZnO NPs-1% rGO composites and reported zinc oxide/graphene nanocomposite sensors in recent literature is summarized in Table 2. ZnO NPs-1% rGO composites have good room temperature gas sensing performance for

NO$_2$ gas and still show good repeatability and selectivity at low NO$_2$ gas concentrations. It can be used as a gas-sensitive material for NO$_2$ detection at room temperature to meet practical applications.
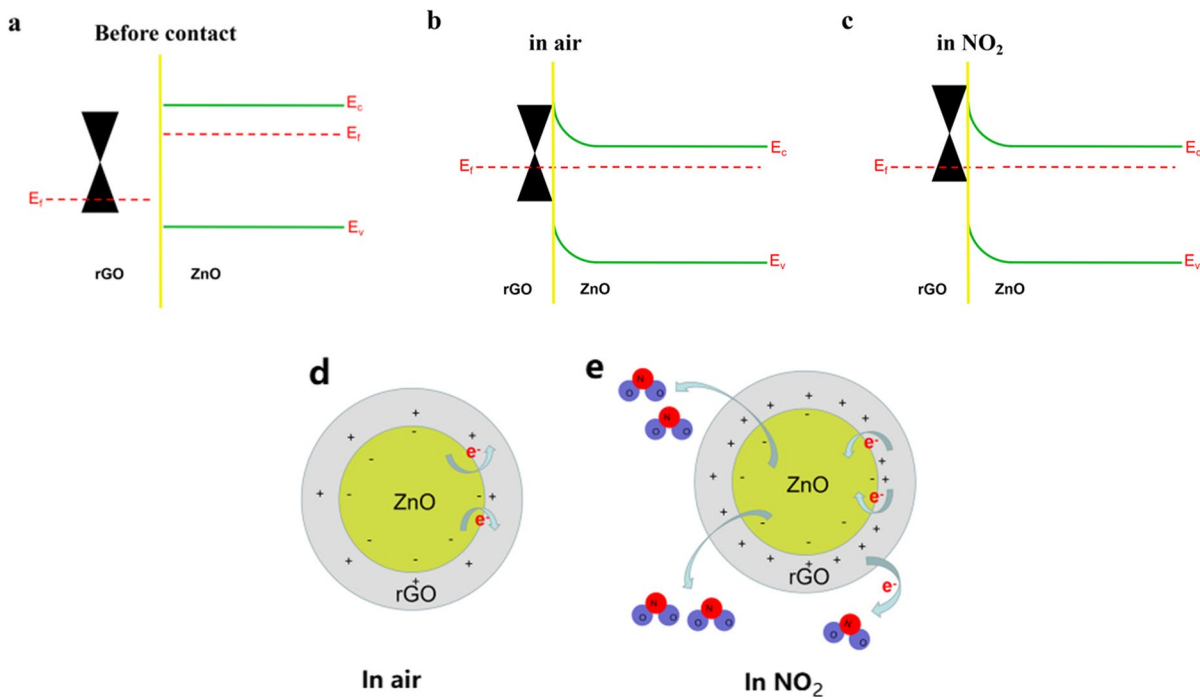
Gas sensing mechanism

In this work, ZnO/rGOs showed P-type responses similar to those of rGO. rGO with an outstanding electric conductivity offers a conductive path. However, the gas-sensitive performance of ZnO/rGO composites does not improve monotonously with increasing rGO content. ZnO played a non-negligible role in contributing to the high responses of the materials. When the ZnO and rGO contact, a unique porous structure is formed, and the specific surface of ZnO/rGO became higher than that of ZnO (Table 1), which facilitated the diffusion of gas [32–34]. Furthermore, a p-n heterojunction forms at the interface, which can benefit the sensing performance [35, 36]. As shown in Scheme 1, the electron flows from n-type ZnO to p-type rGO due to the difference in work function (Scheme 1a) [37–39], which results in a decrease in the carrier concentration (electron/
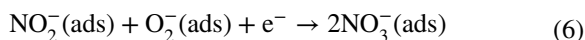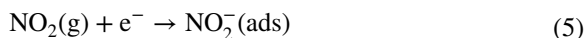
Table 2 The summary of ZnO/rGO composites

Sensing materials	Concentration (ppm)	Temperature (℃)	Sensitivity	Response time/recovery time	Reference
ZnO-rGO (p)film	100	RT	47.4% ($\Delta R/R_a$)	6.2 min/15.5 min	[27]
rGO-ZnO nanoparticles (p)	5	RT	25.6% ($\Delta R/R_a$)	165 s/499 s	[28]
3D graphene aerogel-ZnO (P)	50	RT	8% ($\Delta R/R_a$)	-/-	[29]
Urchin-like nanorods/graphene (p)	100	175	17.4% ($\Delta R/R_a$)	13 min/17 min	[30]
ZnO nano wall/rGO nanosheet	50	RT	9.61 (R_g/R_a)	25 s/15 s	[31]
ZnO NPs-rGO	10	RT	5.21 (R_g/R_a)	198 s/144 s	This work

Scheme 1 **a–e** Gas sensing mechanism of ZnO/rGO in air and in NO$_2$ gas

hole) and an increase in the resistance of ZnO/rGOs. In addition, an internal electrical field is formed. Under air conditions (Scheme 1b and d), oxygen molecules are adsorbed on the surface of the ZnO/rGOs and ionized into oxygen ions (Eq. (3)), capturing electrons from the conduction band of ZnO, which caused an increase in the ZnO electron depletion layer and upward band bending. Upon exposure to NO_2 (Scheme 1c and e), the electron transfers from ZnO/rGOs to the adsorbed NO_2 (Eq. (4)) [40–43]. Since the electronegativity of NO_2^- (ads) is higher than that of O_2^- (ads), they react to form NO_3^- (ads) (Eq. (5)). The reduction of free electrons leads to a larger difference between E_c and E_f in ZnO, weakening the internal electrical field. The electrons in rGO will be transferred to ZnO in the NO_2 environment to increase the holes of rGO. Beside, electrons of rGO are also transferred to NO_2, which further decreases Rg of ZnO/rGOs [44]. Therefore, they exhibit excellent NO_2 sensing properties ($S = $ Ra/Rg) [45–47]. In summary, the excellent gas sensing properties of the ZnO/rGOs are achieved by synergistic effect of the appropriate doping ratio ZnO/rGO composites, as well as their high specific surface area and unique porous structure.

$$O_2(g) + 2e^- \rightarrow 2O_2^-(ads) \tag{4}$$

$$NO_2(g) + e^- \rightarrow NO_2^-(ads) \tag{5}$$

$$NO_2^-(ads) + O_2^-(ads) + e^- \rightarrow 2NO_3^-(ads) \tag{6}$$

Conclusions

In summary, a hybrid material, ZnO/rGO, was successfully synthesized through a facile hydrothermal process. The ratio of rGO in ZnO/rGO had a great effect on the gas sensing behavior. We observed that the ZnO NPs-1% rGO sensor exhibits the highest gas response of 5.21 in 10 ppm NO_2 at room temperature among all gas sensors. The enhanced gas sensing performance is attributed to the enlarged specific surface area of the smaller nanoparticles for more active adsorption sites and the formation of p-n heterojunctions. Our sensors are attractive due to their low energy consumption, simplified sensor manufacturing without heating elements, and low cost.

Declarations

Conflict of interest The authors declare no competing interests.

References

1. Zampolli S, Elmi I, Ahmed F, Passini M, Cardinali GC, Nicoletti S, Dori L (2004) An electronic nose based on solid-state sensor arrays for low-cost indoor air quality monitoring applications. Sens Actuators, B Chem 101:39–46

2. Cui J, Wang D, Xie T, Lin Y (2013) Study on photoelectric gas-sensing property and photogenerated carrier behavior of Ag–ZnO at the room temperature. Sens Actuators, B Chem 186:165–171

3. Li Y, Gong J, He G, Deng Y (2012) Enhancement of photoresponse and UV-assisted gas sensing with Au decorated ZnO nanofibers. Mater Chem Phys 134:1172–1178

4. Burgues J, Hernandez V, Lilienthal AJ, Marco S (2020) Gas distribution mapping and source localization using a 3d grid of metal oxide semiconductor sensors. Sensors and Actuators 304:127309

5. Sun D, Luo Y, Debliquy M, Zhang C (2018) Graphene-enhanced metal oxide gas sensors at room temperature: a review. Beilstein J Nanotechnol 9:2832–2844

6. Huang L, Wang Z, Zhang J, Pu J, Lin Y, Xu S, Shi W (2014) Fully printed, rapid-response sensors based on chemically modified graphene for detecting NO_2 at room temperature. ACS Appl Mater Interfaces 6:7426–7433

7. Li J, Zhang W, Sun J (2016) Enhanced NO_2 detection using hierarchical porous ZnO nano flowers modified with graphene. Ceram Int 42:9851–9857

8. Shafiei M, Bradford J, Khan H, Piloto C, Wlodarski W, Li Y, Motta N (2018) Low-operating temperature NO_2 gas sensors based on hybrid two-dimensional SnS_2-reduced graphene oxide. Appl Surf Sci 462:330–336

9. Zhang D, Liu J, Xia B (2016) Nitrogen dioxide-sensing properties at room temperature of metal oxide-modified graphene composite via one-step hydrothermal method. J Electron Mater 45:4324–4330

10. Singh AK, Uddin MA, Tolson JT, Maire-Afeli H, Sbrockey N, Tompa GS, Koley G (2013) Electrically tunable molecular doping of graphene. Appl Phys Lett 102:043101

11. Huang L, Fan H (2012) Room-temperature solid-state synthesis of ZnO/α-Fe_2O_3 hierarchical nanostructures and their enhanced gas-sensing properties. Sens Actuators, B Chem 171–172:1257–1263

12. Gu F, Nie R, Han D, Wang Z (2015) In_2O_3–graphene nanocomposite based gas sensor for selective detection of NO_2 at room temperature. Sens Actuators, B Chem 219:94–99

13. Niu F, Tao LM, Deng YC, Wang QH, Song WG (2014) Phosphorus doped graphene nanosheets for room temperature NH_3 sensing. New J Chem 38:2269

14. Zhou L, Shen F, Tian X, Wang D, Zhang T, Chen W (2013) Stable Cu_2O nanocrystals grown on functionalized graphene sheets and room temperature H_2S gas sensing with ultrahigh sensitivity. Nanoscale 5:1564

15. Srivastava S, Jain K, Singh VN, Singh S, Senguttuvan TD (2012) Faster response of NO_2 sensing in graphene–WO_3 nanocomposites. Nanotechnology 23:205501

16. Wang Z, Jia Z, Li Q, Zhang X, Sun W, Sun J, Ha B (2018) The Enhanced NO_2 sensing properties of SnO_2 nanoparticles/reduced graphene oxide composite. J Colloid Interface Sci 537:228–237

17. Hosseini ZS, Mortezaali A, Irajizad A, Fardindoost S (2015) Sensitive and selective room temperature H_2S gas sensor based on Au sensitized vertical ZnO nanorods with flower-like structures. J Alloy Compd 628:222–229

18. Ahmad R, Tripathy N, Ahn MS, Hahn YB (2017) Highly stable hydrazine chemical sensor based on vertically aligned ZnO nanorods grown on electrode. J Colloid Interface 494:153–158

19. Gao H, Ma Y, Song P, Leng J, Wang Q (2021) Gas sensor based on rgo/ZnO aerogel for efficient detection of NO_2 at room temperature. J Mater Sci: Mater Electron 32:10058–10069

20. Randeniya LK, Shi H, Barnard AS, Fang J, Martin PJ, Ostrikov KK (2013) Harnessing the influence of reactive edges and defects of graphene substrates for achieving complete cycle of room-temperature molecular sensing. Small 9:3993–3999

21. Lee YR, Huang JX, Lin JC, Lee JR (2017) Study of the substrate-induced strain of as-grown graphene on Cu(100) using temperature-dependent raman spectroscopy: estimating the mode Grüneisen parameter with temperature. J Phys Chem C 121:27427–27436

22. Yan P, Liu J, Yuan S, Liu Y, Cen W, Chen Y (2018) The promotion effects of graphitic and pyridinic N combinational doping on graphene for ORR. Appl Surf Sci 445:398–403

23. Thamer A, Faisal A, Abed A, Khalef W (2020) Synthesis of gold-coated branched ZnO nanorods for gas sensor fabrication. J Nanopart Res 22:74

24. Alosfur FKM, Ridha NJ (2021) Synthesis and characterization of ZnO/SnO2 nanorods core–shell arrays for high performance gas sensors. Appl Phys A 127:203

25. Leonard KC, Nam KM, Lee HC, Kang SH, Bard AJ (2013) $ZnWO_4$/WO_3 composite for improving photoelectrochemical water oxidation. J Phys Chem C 117:15901–15910

26. Wang H, Bai J, Dai M, Liu K, Lu G (2019) Visible light activated excellent NO_2 sensing based on 2d/2d ZnO/g-C_3N_4 heterojunction composites. Sens Actuators, B Chem 304:127287

27. Lee HY, Heish YC, Lee CT (2019) High sensitivity detection of nitrogen oxide gas at room temperature using zinc oxide-reduced graphene oxide sensing membrane. J Alloy Compd 773:950–954

28. Liu S, Yu B, Zhang H, Fei T, Zhang T (2014) Enhancing NO_2 gas sensing performances at room temperature based on reduced graphene oxide-ZnO nanoparticles hybrids. Sens Actuators, B Chem 202:272–278

29. Liu X, Sun J, Zhang X (2015) Novel 3d graphene aerogel–ZnO composites as efficient detection for NO_2 at room temperature. Sens Actuators, B Chem 211:220–226

30. Jing L, Xin L, Sun J (2015) One step solvothermal synthesis of urchin-like ZnO nanorods/graphene hollow spheres and their NO_2 gas sensing properties. Ceram Int 42:2085–2090

31. Liu Z, Yu L, Guo F, Sheng L, Qi L, Shan M (2017) Facial development of high performance room temperature NO_2 gas sensors based on ZnO nanowalls decorated rgo nanosheets. Appl Surf Sci 423:721–727

32. Moon DB, Bag A, Lee HB, Meeseepong M, Lee DH, Lee NE (2021) A stretchable, room-temperature operable, chemiresistive gas sensor using nanohybrids of reduced graphene oxide and zinc oxide nanorods. Sens Actuators, B Chem 345:130373

33. Wang P, Wang D, Zhang M, Zhu Y, Xu Y, Ma X, Wang X (2016) ZnO nanosheets/graphene oxide nanocomposites for highly effective acetone vapor detection. Sens Actuators, B Chem 230:477–484

34. Gao R, Gao S, Wang P, Xu Y, Huo L (2020) Ionic liquid assisted synthesis of snowflake ZnO for detection of nox and sensing mechanism. Sens Actuators, B Chem 303:127085

35. Meng F, Chang Y, Qin W, Yuan Z, Zhao J, Zhang J (2019) ZnO-reduced graphene oxide composites sensitized with graphitic carbon nitride nanosheets for ethanol sensing. ACS Appl Nano Mater 2:2734–2742

36. Wu XL, Siu GG, Fu CL, Ong HC (2001) Photoluminescence and cathodoluminescence studies of stoichiometric and oxygen-deficient ZnO films. Appl Phys Lett 78:2285–2287

37. Minh Triet N, Thai Duy L, Hwang BU, Hanif A, Siddiqui S, Park KH, Lee NE (2017) High-performance Schottky diode gas sensor based on the heterojunction of three-dimensional nanohybrids of reduced graphene oxide–vertical ZnO nanorods on an AlGaN/GaN layer. ACS Appl Mater Interfaces 9:30722–30732

38. Qu G, Fan G, Zhou M, Rong X, Chen D (2019) Graphene-modified ZnO nanostructures for low-temperature NO_2 sensing. ACS Omega 4:4221–4232

39. Sonker RK, Sabhajeet SR, Singh S, Yadav BC (2015) Synthesis of ZnO nanopetals and its application as NO_2 gas sensor. Mater Lett 152:189–191

40. Ou JZ, Ge W, Carey B, Daeneke T, Rotbart A, Shan W, Kalantar-zadeh K (2015) Physisorption-based charge

transfer in two-dimensional SnS_2 for selective and reversible NO_2 gas sensing. ACS Nano 9:10313–10323

41. Guo W, Zhao B, Zhou Q, He Y, Wang Z, Radacsi N (2019) Fe-doped ZnO/reduced graphene oxide nanocomposite with synergic enhanced gas sensing performance for the effective detection of formaldehyde. ACS Omega 4:10252–10262

42. Wang Z, Gao S, Fei T, Liu S, Zhang T (2019) The construction of ZnO/SnO_2 heterostructure on reduced graphene oxide for enhanced nitrogen dioxide sensitive performances at room temperature. ACS sensors 4:2048–2057

43. Balucani M, Nenzi P, Chubenko E, Klyshko A, Bondarenko V (2011) Electrochemical and hydrothermal deposition of ZnO on silicon: from continuous films to nanocrystals. J Nanopart Res 13:5985–5997

44. Naa A, Kampara RK, PK R, JB G, (2018) Highly sensitive graphene oxide functionalized ZnO nanowires for ammonia vapor detection at ambient temperature. Sens Actuators, B Chem 255:1064–1071

45. Wang H, Zhou L, Liu Y, Liu F, Liang X, Liu F, Lu G (2019) UV-activated ultrasensitive and fast reversible ppb NO_2 sensing based on ZnO nanorod modified by constructing interfacial electric field with In_2O_3 nanoparticles. Sens Actuators, B Chem 305:127498

46. Xia Y, Wang J, Xu JL, Li X, Xie D, Xiang L, Komarneni S (2016) Confined formation of ultrathin ZnO nanorods/reduced graphene oxide mesoporous nanocomposites for high-performance room-temperature NO_2 sensors. ACS Appl Mater Interfaces 8:35454–35463

47. Drmosh QA, Hendi AH, Hossain MK, Yamani ZH, Moqbel RA, Hezam A, Gondal MA (2019) UV-activated gold decorated rGO/ZnO heterostructured nanocomposite sensor for efficient room temperature H_2 detection. Sens Actuators, B Chem 290:666–675